PERGAMON

Journal of Structural Geology 22 (2000) 811–829

JOURNAL OF STRUCTURAL GEOLOGY

www.elsevier.nl/locate/jstrugeo

# Hydrologic segmentation of high-temperature shear zones: structural, geochemical and isotopic evidence from auriferous mylonites of the Renco mine, Zimbabwe

Alexander F.M. Kisters[a,*], Jochen Kolb[a], F. Michael Meyer[a], Stephan Hoernes[b]

[a]*Institut für Mineralogie und Lagerstättenlehre, Aachen University of Technology (RWTH), Wüllnerstr. 2, D-52056 Aachen, Germany*
[b]*Mineralogisch Petrologisches Institut, Poppelsdorfer Schloß, D-53115 Bonn, Germany*

Received 5 March 1999; accepted 20 January 2000

**Abstract**

Combined structural, mineralogical and geochemical observations in auriferous mylonites of the Renco mine, hosted by late-Archaean, high-grade metamorphic granitoids in southern Zimbabwe, are used to describe the spatially heterogeneous fluid flow and metasomatism that occurred synchronous with deformation at mid- to upper-amphibolite facies metamorphic conditions. Significantly, the narrow (on average 1m-wide) mylonitic shear zones are internally zoned reflecting a pronounced hydrologic segmentation during deformation. Shear zones typically consist of two distinct domains: (i) anastomosing, quartz–feldspar–biotite–hornblende mylonites and/or quartz mylonites, and (ii) tabular-shaped pods, referred to as lithons, that are enveloped by mylonites and that exhibit evidence of transient episodes of brittle fracturing and ductile creep. Whole-rock geochemistry and mass balance calculations indicate dramatic element, volume (up to $\geq 100\%$) and associated mass gains for the brittle–ductile lithons that are mineralogically reflected in a volumetrically abundant sulphide mineralisation and the formation of a pervasively developed silicate alteration paragenesis. In contrast, mylonites have experienced only minor element and volumetric changes and minor alteration. $\delta^{18}O$ values for whole rocks and quartz are enriched in lithons compared to wall rocks and enveloping mylonites, which implies the influence of externally derived fluids.

These results indicate a strongly domainal fluid flow and mass transfer. Fluid advection was dominated by microscopic and macroscopic fracture permeabilities related to periods of coseismic dilatancy in lithons. The patchy, but partly interconnected distribution of lithons enveloped by mylonites indicates that deformation in the high-temperature shear zones was characterised by transient periods of seismic slip rather than continuous aseismic creep. Based on the well-preserved internal mineralogical and textural development of the Renco shear zones a more general model applicable for fluid advection coupled with the rheological behaviour of mid-crustal shear zones is presented. 

## 1. Introduction

Fault zones at all crustal levels represent potentially high-permeability fluid conduits that may record large fluid fluxes compared to their wall rocks (Marquer and Burkhard, 1992; Dipple and Ferry, 1992; Marquer et al., 1994; Goddard and Evans, 1995; McCaig, 1997). Fluid flow is commonly associated with material transport and considerable volume and mass changes related to fluid infiltration have been documented (O'Hara, 1988; O'Hara and Blackburn, 1989; Selverstone et al., 1991). The fluid-flow properties and, consequently, also the rheology of fault rocks are greatly influenced by the variability and spatial and temporal relationships of different deformation mechanisms that accommodate strain in faults and shear zones (Cox and Etheridge, 1989; O'Hara, 1990; Marone et al., 1990; Tobisch et al., 1991; Blanpied et al., 1992, 1995; Evans and Chester, 1995; Marone, 1998). The efficiency of fluid flow in shear zones of mid- and lower-

* Present address: Department of Geology, University of Stellenbosch, Private Bag X1, 7602, Matieland, South Africa.
*E-mail address:* akisters@land.sun.ac.za (A.F.M. Kisters).

0191-8141/00/$ - see front matter 
PII: S0191-8141(00)00006-7

crustal levels is largely determined by the interplay of two competing processes, namely (1) pore compaction during ductile creep or the closure of pores due to the precipitation of hydrothermal minerals during fluid flow, and (2) the creation of porosities and, if suitably interconnected, permeabilities during transient episodes of microfracturing. Although the two processes appear to be counteractive at first sight, it is well established that microfracturing at deeper crustal levels can, under reasonable geological strain rates, only occur if pore fluid pressures are increased to close-to lithostatic levels as a result of compaction and crystal-plastic deformation (Etheridge, 1983; Etheridge et al., 1984; Sibson, 1986, 1994). There is now increasing evidence that the development of porosity networks in high-temperature 'ductile' shear zones is dominated by the episodic interconnection of microscopic and mesoscopic intergranular cracks and fractures (Knipe and McCaig, 1994; McCaig, 1997; Mancktelow et al., 1998). Moreover, recent work on brittle and brittle–ductile shear zones has shown that the permeability structure of faults may be highly anisotropic and directional due to transient episodes of domainal fracturing and the formation of fluid compartments within faults (Chester et al., 1993; Byerlee, 1993). However, the recognition of the relative contribution of grain-scale permeability vs. microfracturing to the hydraulic properties of natural shear zones is often hampered by the commonly extensive dynamic and static recrystallisation of mineral textures (Knipe and McCaig, 1994). In addition, flow laws that can adequately describe mixed deformation mechanisms in multiphase aggregates of faults and shear zones have not yet been formulated to reasonable degrees of confidence (Sleep and Blanpied, 1992).

In this paper, we combine structural, mineralogical, geochemical, and isotope geochemical data that are used to illustrate the structural controls of fluid advection in amphibolite-facies shear zones. The data were collected from the auriferous shear zone system of the Renco gold mine hosted by granulite-facies enderbites and migmatitic gneisses of the Northern Marginal Zone of the late-Archaean Limpopo Belt in southern Zimbabwe (Blenkinsop and Frei, 1996; Kisters et al., 1998). A pervasive alteration paragenesis, sulphide mineralisation, and economic-grade gold mineralisation confined to the narrow shear zones testify to the extensive, strongly channelled fluid flow and material transport. We present new observations on the microscopic, mesoscopic and mine-scale development of fabrics, mineralogic alteration, fluid–rock interaction and isotope signatures that (1) preserve an excellent record of the complex fluid channelling and three-dimensional geometry of fluid pathways in the mid-crustal shear zones, and (2) provide evidence of massive volume and associated mass gains reflecting extensive, probably far-field, fluid infiltration. The observations are used to formulate a conceptual model of structurally controlled fluid flow at mid-crustal levels. We also suggest that the mechanisms of permeability enhancement described here are more widespread in ductile shear zones, but that evidence may be overprinted in many high-temperature shear zones during longer periods of ductile creep, recrystallisation, and the lack of obvious fracturing events in the absence of mineralogically distinct veins.

## 2. Geological setting and mine geology

The Renco gold mine is located in heterogeneously deformed granulite-grade enderbites and migmatitic gneisses that form part of a moderate southerly dipping, up to 5-km-wide thrust zone, the North Limpopo Thrust Zone (NLTZ; Blenkinsop et al., 1995). The NLTZ separates high-grade metamorphic, mainly plutonic assemblages of the Northern Marginal Zone of the Limpopo Belt to the south from low- to medium-grade granite–greenstone terrains of the Zimbabwe craton in the north (Fig. 1) (Ridley, 1992; Mkweli et al., 1995). NNW-directed thrusting of the granulite-facies plutonic rocks of the Northern Marginal Zone onto the Zimbabwe craton occurred during late-Archaean tectonics at ca. 2.6 Ga under granulite- to amphibolite-facies conditions (Mkweli et al., 1995; Berger et al., 1995; Kamber et al., 1995).

Gold and associated sulphide mineralisation at the Renco Mine is confined to a series of narrow mylonitic shear zones, locally referred to as 'reefs' (Tabeart, 1989; Blenkinsop and Frei, 1996; Kisters et al., 1998). On a mine scale, two different shear zone geometries and orientations can be distinguished. These include a set of anastomosing, shallow southeasterly dipping subparallel shear zones ('shallow reefs'), and E–W-trending, steep to subvertically dipping shear zones ('steep reefs') (Fig. 2). The orientation of the reef structures and shear sense indicators imply that the auriferous shear zones represent second-order structures related to the late-Archaean, NNW-directed thrusting of the NMZ onto the Zimbabwe craton (Ridley, 1992; Kisters et al., 1997a, 1998).

Temperatures during deformation in the auriferous shear zones can be constrained by stable isotope thermometry and geothermometry on synkinematic alteration parageneses (Kolb et al., 2000). Stable isotope thermometry indicates temperatures of 640–710°C during deformation, testifying to mid- to upper-amphibolite-facies conditions of deformation. Geothermometry on garnet–biotite mineral pairs (after Ferry and Spear, 1978) from the shear zones yields temperatures of 580–630°C (Kisters et al., 1998). These values, however, have to be taken as minimum estimates, since garnet and biotite tend to re-equilibrate at lower

temperatures of 580–600°C (Spear and Peacock, 1992). Similar temperatures of ca. 680°C based on geothermometry on orthopyroxene–garnet rims from sheared enderbites of the Renco wall rocks were obtained by Rollinson (1989). The temperature estimates for deformation in the auriferous reefs correlate with temperatures given for the widespread amphibolite-facies retrogression of granulite wall rocks during late-Archaean thrust tectonics for which $P$–$T$ conditions of $P$ = ca. 400 MPa and $T$ = ca. 650°C were calculated by Tsunogae et al. (1992) and Ridley (1992).

The presence of an economic-grade gold and volumetrically abundant sulphide mineralisation together with the formation of pervasive alteration mineral parageneses confined to the reef structures provides compelling evidence that deformation in the shear zones was associated with extensive fluid advection (Tabeart, 1989; Kisters et al., 1997a, 1998). Kolb et al. (2000) have recently used mineral equilibria of ore and alteration parageneses, isotope and fluid inclusion studies to constrain the nature of the fluid responsible for mineralisation and alteration in the high-temperature shear zones. Their work indicates that the fluid was of a mixed $CO_2$–$H_2O \pm CH_4 \pm N_2$ composition, moderately oxidised (log $f_{O2}$ $10^{-17}$–$10^{-18}$ bars) with high $a_{H2S}$ of 0.25–0.75 (calculated for $T$ = 600°C and $P$ = 400 MPa). High $a_{H2S}$ of the fluid readily explains the abundance of sulphides in the reefs, which, as discussed below in detail, are used to delineate the fluid pathways within the shear zones.

Both wall rocks and reef structures are affected by a lower greenschist-facies retrogression (Blenkinsop and Frei, 1996; Kisters et al., 1998). The retrogression is pervasive within and in proximity to brittle faults that cut the high-grade reef structures, but is only subordinate away from the breccia zones. The petrographic descriptions and geochemical analyses presented in this study refer to samples not affected by the late, greenschist-facies overprint.

## 3. Mesoscopic and microscopic description of the reef structures

### 3.1. Internal shear zone structure

Auriferous shear zones of the Renco mine are, on average, 1 m wide, but may locally attain maximum widths of up to 3 m. They show a tabular-shaped, slightly undulating geometry and are hosted by weakly

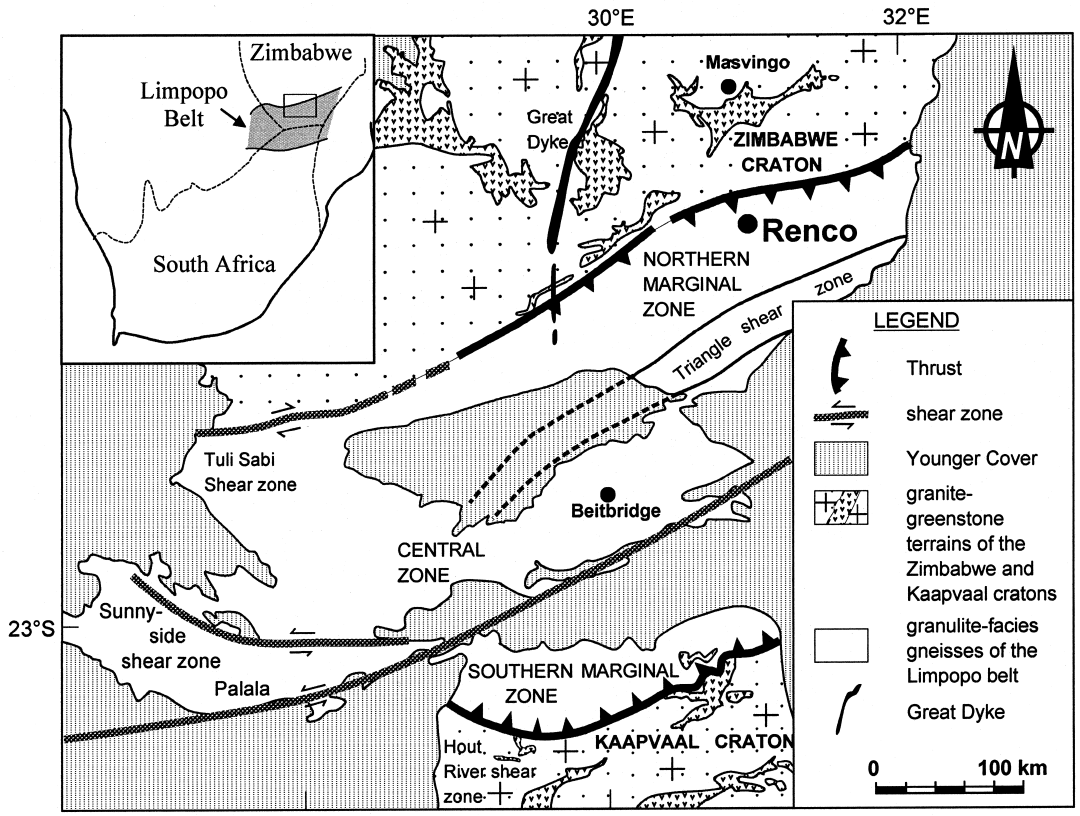


Fig. 1. Simplified geological map of the Limpopo Belt in southern Africa, showing the location of the Renco mine in the Northern Marginal Zone in close proximity to the main thrust zone (North Limpopo Thrust Zone: NLTZ), which separates the Zimbabwe Craton in the north from the Limpopo Belt in the south (modified after Blenkinsop and Rollinson, 1992).

deformed to massive, high-grade metamorphic enderbites and migmatitic gneisses. In detail, the shear zones exhibit a complex internal structure both on an outcrop- and a mine scale, comprised of mineralogically and structurally distinct domains that indicate that both crystal-plastic deformation and brittle fracturing were significant during shearing. These two domains include (1) fine-grained to banded anastomosing mylonites, including quartz–feldspar–biotite–hornblende mylonites and, locally, almost monomineralic quartz (±feldspar) mylonites; and (2) lenticular- to tabular-shaped pods enclosed by the mylonites, henceforth referred to as *lithons,* that show brittle–ductile fabrics, a volumetrically abundant sulphide mineralisation and pervasive silicate alteration paragenesis (Fig. 3a–c). It should be emphasised that the terms 'lithon' and 'mylonite' in the present study are not used to denote zones of low and high finite strain since there are no reliable strain markers in the auriferous shear zones, but are only used to contrast different deformational styles and strain histories of the two domains.

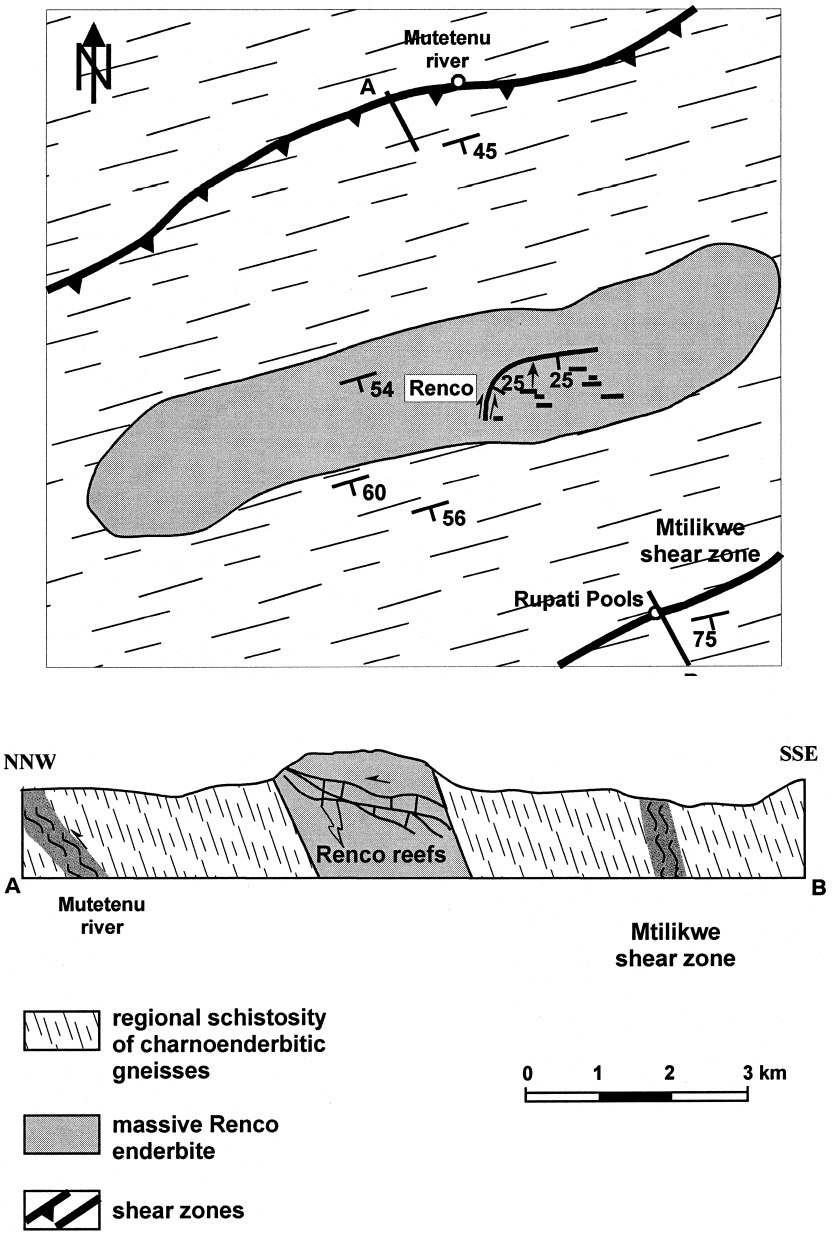


Fig. 2. (a) Schematic geological map showing the location of the Renco mine hosted by relatively weakly deformed enderbites and migmatitic gneisses of the Renco enderbite. The Renco enderbite is surrounded by southerly dipping enderbitic and charnockitic gneisses that form part of the North Limpopo Thrust Zone (modified after Ridley, 1992); (b) Simplified cross-section illustrating the occurrence of the two sets of auriferous shear zones within the Renco enderbite.

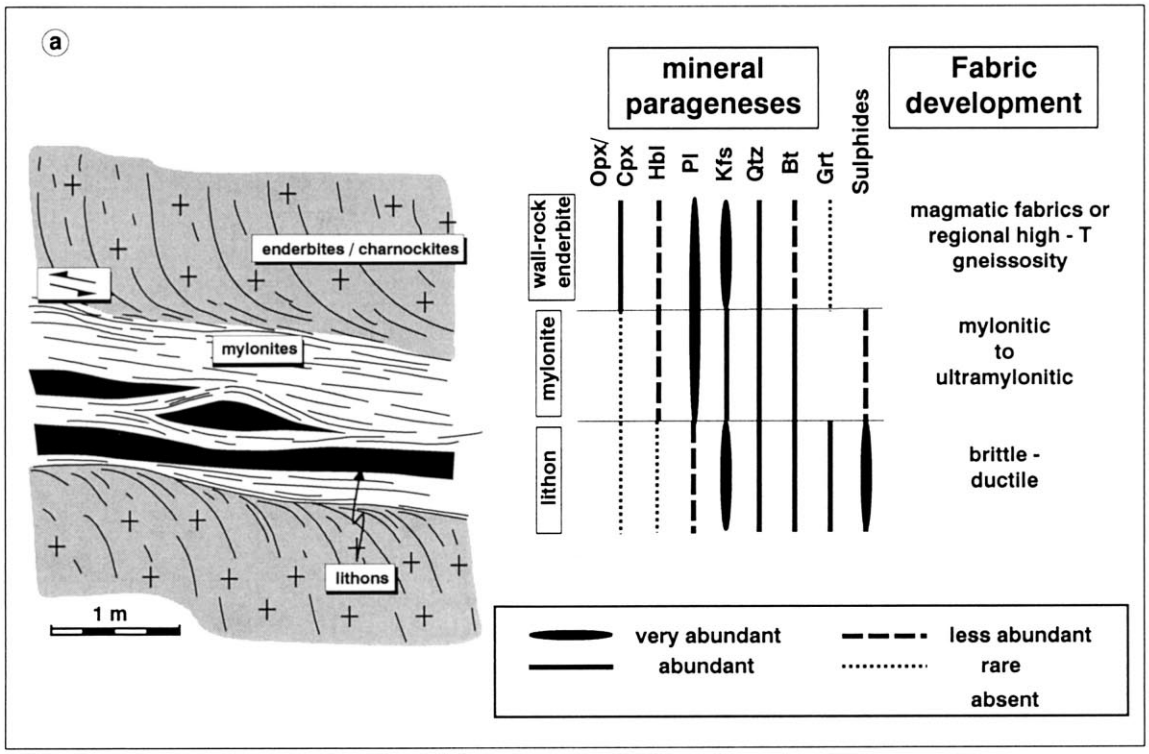


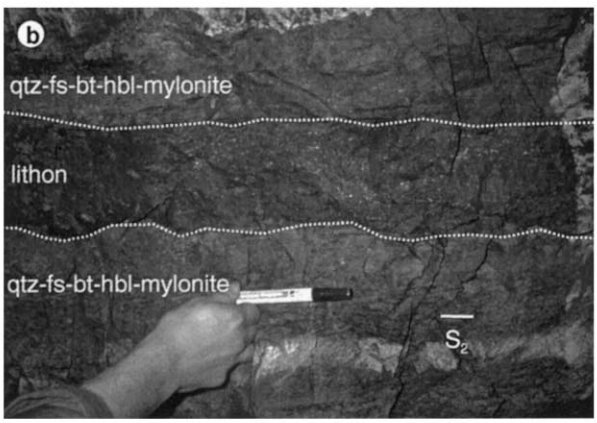


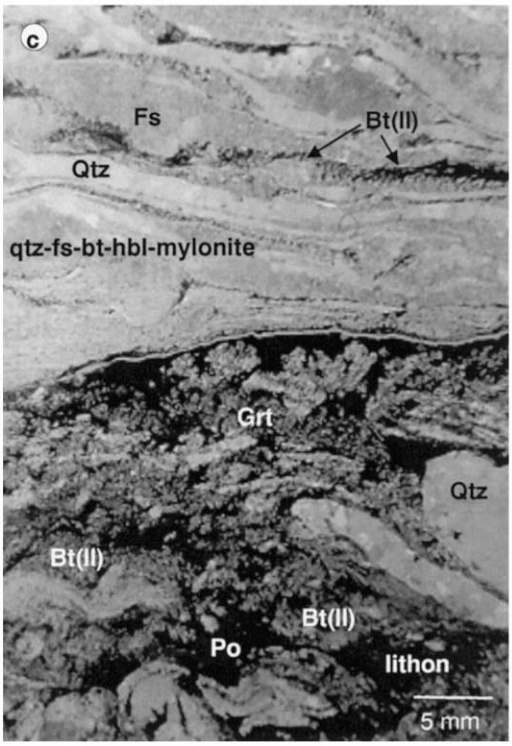


Fig. 3. (a) Schematic cross-section through the reef structures of the Renco mine, showing the main lithotypes, namely mylonites and lithons bounded by massive wall-rock enderbites. Shearing in the reefs is accompanied by marked changes in the mineralogy of various lithotypes and a distinct fabric development in different lithotypes; (b) Underground exposure of a lithon sandwiched between quartz–feldspar–biotite–hornblende mylonites; S2: mylonitic foliation; note the marked colour contrast between the lithon and mylonites due to the different mineralogic composition, and the sharp contact between the two domains (highlighted by dotted line). (c) Thin section (in plane polarised light) of the contact between mylonites (upper half of the photo) and a lithon (lower half of the photo). Mylonites are composed of quartz ribbons (qtz), feldspar (fs) and biotite (II), while lithons contain sulphides (po: pyrrhotite) that occur in veinlets, garnet (medium-grey euhedral to rounded aggregates), biotite (II), quartz and alkali feldspar (fine-grained, light).

### 3.2. Distribution of mylonites and lithons in shear zones

Mylonites typically form an anastomosing, three-dimensional network within the shear zones. Individual mylonite bands in the shear zones range in width from $\leq 1$ cm to $\geq 15$ cm, but, in places, mylonitisation may have also affected the entire reef structure. The geometry of this network is determined by the branching-and-coalescing outcrop pattern of mylonites that can be mapped both in an up-dip direction and along strike of the shear zones. The three-dimensional outcrop pattern of the mylonite network determines the occurrence and spatial distribution of lithons that occur as tabular-shaped, parallel-sided lenses enveloped by mylonites (Figs. 3a, b and 4). Contacts between mylonites and lithons are commonly sharp (Fig. 3b). Both up-dip and strike extents of lithons vary from 1–2 m to several tens of metres (max. ca. 50 m). The width of lithons ranges from $\leq$ 1 cm to $\geq$ 50 cm. In places up to five foliation-parallel lithons separated by thin mylonite bands can be observed within the narrow shear zones, but wider lithons may also occupy almost the entire width of the reef structures. Significantly, narrow lithons may coalesce to form wider lithons, particularly in an up-dip direction, but depending on the geometry of the enclosing mylonites, they may also pinch within a few metres both along strike and in an up-dip direction. Thus, lithons in the underground workings of the mine form an at least partly interconnected three-dimensional network contained within the mylonitic shear zones (Fig. 4).

In the following we will describe the petrographic and structural development of the two distinct domains together with the bounding wall-rock enderbites.

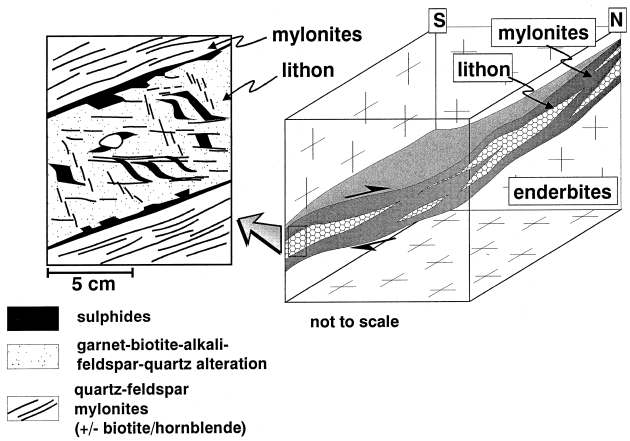


Fig. 4. Schematic sketch of a reef structure hosted by enderbites illustrating the pod-like, irregular distribution and occurrence of lithons in mylonitic shear zones of the Renco mine. Note that the thickness of the mylonitic shear zones is greatly exaggerated. Inset (left) shows the spatial relationship between ductile mylonites and brittle–ductile lithons on the scale of a hand-specimen (compare Fig. 3b).

### 3.3. Petrography and textural development of lithotypes

Wall-rock enderbites are typically massive to weakly foliated, medium-grained rocks that may also include migmatitic varieties such as stromatic or schollen-and-raft migmatites. The rocks are principally made up of quartz, plagioclase, alkali feldspar, orthopyroxene, biotite, and accessory garnet, clinopyroxene, green hornblende, apatite, zircon and opaques. Magmatic textures testify to the intrusive nature of the enderbites being emplaced as large plutonic complexes into mid- to lower-crustal levels (Ridley, 1992). Grain sizes in undeformed enderbites commonly range from 1 mm to 5 mm and, locally, up to 15 mm. In proximity to the reef structures (i.e. within approximately 0.5 m of the shear zones), primary orthopyroxene is replaced by retrograde hornblende and/or biotite and a gradual strain increase into the sheared reefs is indicated by the dynamic recrystallisation of minerals.

Mylonitic rock types within the reef structures comprise protomylonites and mylonites. Texturally, mylonites are characterised by crystal-plastic deformation and a grain-size reduction by one to two orders of magnitude compared to undeformed enderbites, to grain sizes of 0.1–0.02 mm. The mylonites are composed of recrystallised quartz (II), plagioclase (II) and alkali feldspar (II) together with biotite (II) and minor hornblende (II). A well-developed foliation is defined by ribbon-quartz aggregates, bands of finely recrystallised feldspar and foliation-parallel biotite (bt II) (Fig. 3c). Quartz and quartz–feldspar aggregates define a mineral stretching lineation, which shows shallow southerly plunges in shallow reefs. Mechanisms of recrystallisation of quartz are grain-boundary migration and subgrain rotation. Grain boundaries between quartz and feldspar are, in places, strongly lobate indicating diffusion creep. Feldspars occur as either ovoid-to-rounded mantled porphyroclasts (plg I and kfs I) or they may be completely recrystallised to yield fine-grained bands parallel to quartz ribbons that define the mylonitic foliation. Recrystallisation of feldspar occurred mainly due to subgrain rotation. Locally, feldspar (II) shows myrmekitic textures. Mantles of feldspar porphyroclasts consist of aggregates of fine-grained feldspar (II)–quartz (II)–biotite (II) + opaques (mainly pyrrhotite) (Fig. 5a). Quartz–feldspar–biotite–hornblende mylonites grade laterally into quartz-rich mylonites that also contain rounded feldspar porphyroclasts and minor opaques. Mechanisms of recrystallisation in quartz mylonites are similar to those of quartz–feldspar–biotite–hornblende mylonites. However, recrystallisation of quartz is more prominent and quartz grains display a pronounced crystallo-

graphic preferred orientation. In both quartz mylonites and quartz–feldspar–biotite–hornblende mylonites, quartz may display an annealed microstructure with largely strain free quartz grains, straight grain boundaries decorated with fluid inclusions and approximately 120° triple junctions between adjacent grains. Locally, large older quartz grains still preserve evidence of undulose extinction and subgrain formation.

Lithons represent tabular-shaped lenses enclosed by mylonites that display less crystal-plastic deformation than surrounding mylonites, but in which mineralogic alteration and micro- and mesoscale veining dramatically increase compared to enveloping mylonites and wall-rock enderbites. Neomineralisation and alteration in lithons occur in form of veins and in μm- to mm-scale breccia zones mainly healed by sulphides, and more pervasively as an extensive silicate alteration mineral assemblage. Vein filling, brecciated material and the silicate alteration parageneses constitute up to 90 vol.% of lithons and lithons are composed of sulphides (pyrrhotite ≫ chalcopyrite ≥ pyrite), garnet, biotite, quartz, alkali feldspar ± siderite in varying

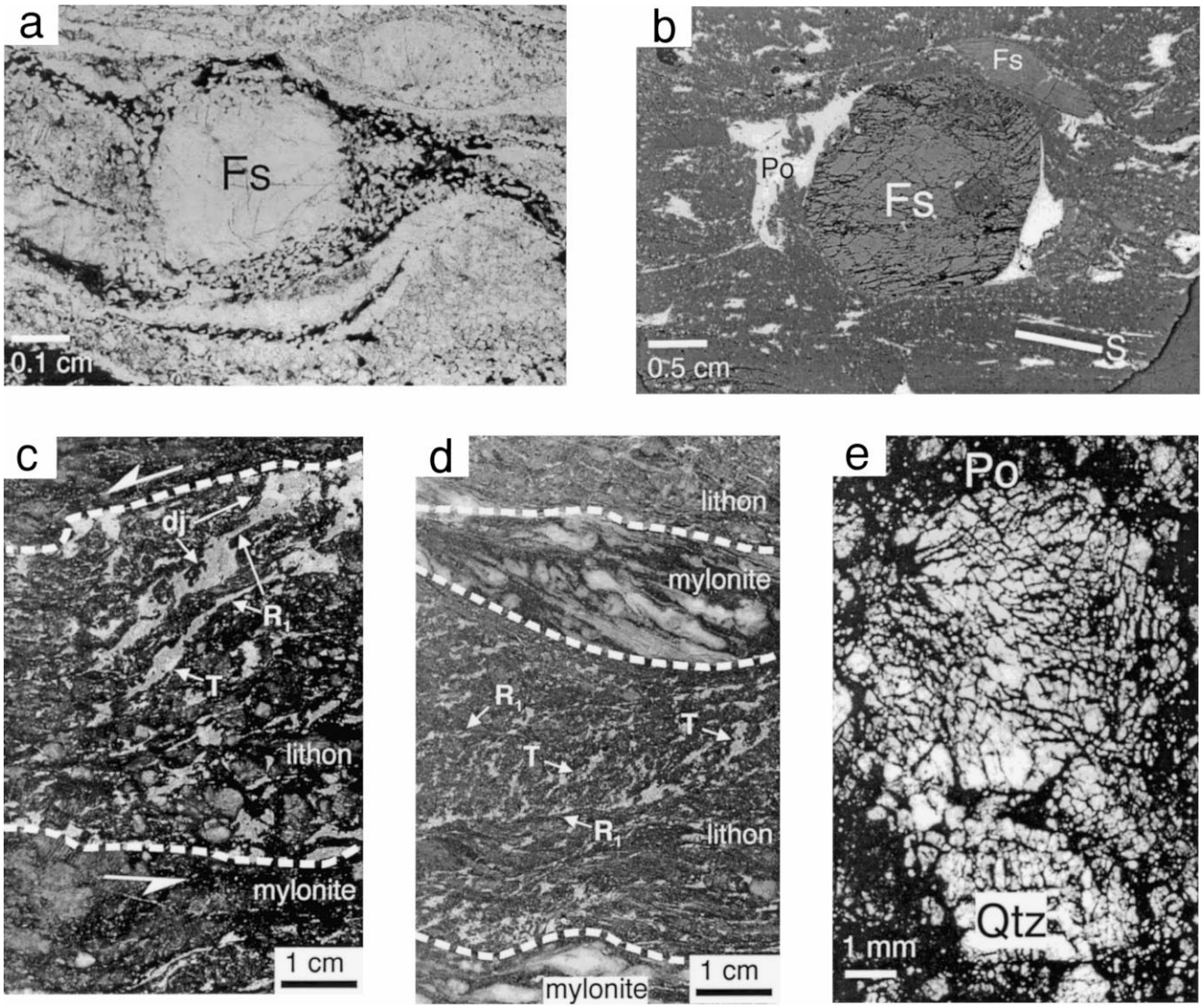


Fig. 5. (a) Photograph of a thin section (plane polarised light) taken from a quartz–feldspar–biotite–hornblende mylonite, showing neomineralisation in the form of biotite (dark flakes) and sulphides (opaque) in the recrystallised mantle of a feldspar porphyroclast (fs). (b) Photograph of a polished section illustrating the precipitation of sulphide (po) in the strain-shadow position around a large feldspar porphyroclast (fs); S denotes the foliation in the mylonite. (c) Photograph of a polished hand-specimen illustrating the occurrence of sulphides (light grey, mainly pyrrhotite and chalcopyrite) along brittle structures including synthetic Riedel shears (R1), tension gashes (T) and dilational jogs (dj) in a lithon sandwiched by mylonite bands. (d) Photograph of a polished hand specimen illustrating the close spatial relationship between ductile fabrics in mylonites and brittle–ductile fabrics in lithons. (e) Photograph of thin section taken from a dilational jog in a lithon illustrating the occurrence of implosion breccias that is evidenced by the mosaic breccia textures displayed by quartz (light, qtz) cemented by sulphides (black, po: pyrrhotite).

amounts (Fig. 3a, c). Brittle fracture networks in lithons consist of different macroscopic and microscopic vein geometries filled with mainly sulphides and, locally, fine specks of free gold. Both texturally and volumetrically, sulphide mineralisation shows a progressive development in lithons from sulphides that occur in isolated high- and low-angle veinlets, through intersecting vein or fracture arrays that are variably folded and sheared. Ultimately, parallel-sided massive sulphide reefs result, which contain up to 75 vol.% sulphides and rounded- to subangular inclusions of wall-rock enderbites or the silicate alteration assemblage. This progressive textural and mineralogical development of lithons is observed both up-dip and along strike of the shear zones.

Ductile deformation in lithons is evidenced by the recrystallisation and grain-size reduction, in particular, of quartz, biotite, and feldspar of the main alteration assemblage. Garnet forms locally rotated porphyroblasts. Biotite defines a foliation parallel to that of the enveloping mylonites, but it may also define an oblique fabric together with recrystallised, slightly elongate grains of quartz. The obliquity of this fabric is consistent with the sense of shear in enveloping mylonites. Feldspar predominantly alkali feldspar, occurs finely recrystallised in the matrix together with quartz and biotite, or as rounded, mantled porphyroclasts. Quartz ribbons in lithons are commonly tightly folded containing sulphides in hinge zones, which are, in turn, truncated by straight or variably folded sulphide-filled fractures. Where ductile shearing has affected sulphides, they occur as flakes strongly drawn out in the plane of the foliation. Undulose extinction, deformation twins, static recrystallisation features and the folding of veins testify to the deformed nature of sulphides and sulphide veinlets.

### 3.4. Permeability structure in mylonites and lithons

Neomineralisation, mainly in the form of sulphides and the formation of alteration minerals, and the occurrence and siting of these mineral phases are used to describe the permeability structure of mylonites and lithons in the reefs. The precipitation of opaques and formation of distinct alteration minerals in mylonites and, particularly, in lithons greatly facilitates the identification of permeabilities in orientated thin and polished sections. However, it should be emphasised that the recrystallisation of mineral textures has probably, at least to a certain degree, modified original permeabilities and that the following description most likely represents only a qualitative account of the total permeability structure during high-temperature deformation and associated fluid flow.

In total, some 200 orientated polished thin sections were examined. Samples were cut parallel to the mineral stretching lineation and perpendicular to the foliation and perpendicular to both the mineral stretching lineation and foliation.

#### 3.4.1. Mylonites

Neomineralisation in mylonites is mainly evidenced by the occurrence of sulphides that are markedly more abundant compared to wall-rock enderbites and the formation of biotite and/or hornblende. Sulphides are mainly fine grained and occur in three main different situations, often closely associated with biotite: (1) in dynamically recrystallised mantles of feldspar porphyroclasts (Fig. 5a), (2) in finely, recrystallised bands within or along the margins of quartz-ribbons or recrystallised feldspars, and (3) in strain-shadow positions around feldspar porphyroclasts with a geometry similar to σ-type porphyroclasts (Fig. 5b). Strongly drawn out flakes of opaques that lie in the plane of the mylonitic foliation testify to the progressive precipitation of sulphides during crystal-plastic deformation. Sulphide-filled fractures transecting the mylonitic foliation at high angles of 75–80° are locally abundant.

#### 3.4.2. Lithons

Lithons are characterised by abundant microscopic and mesoscopic veins (Fig. 5c, d). Tension gash geometries are evident from the angles they enclose (ca. 35–50°) relative to either enveloping mylonites that bound lithons, or with secondary, low-angle synthetic Riedel shears (see below) that are developed within the lithons. The displacement of fractured feldspar porphyroclasts perpendicular to the vein walls indicates that they are essentially extensional (mode I) cracks. The length of the extension fractures ranges from < 10 μm up to 1 cm and their width is between several microns and 3 mm. Tension gashes occur as closely spaced en-échelon veins or as complex, sigmoidally folded vein arrays. In places, a spalling of wall rocks into larger tension gashes can be observed. Wall-rock fragments display angular outlines and are cemented by mainly pyrrhotite. These 'jigsaw-puzzle' like breccias (Fig. 5e) correspond to implosion or mosaic breccias described by e.g. Sibson (1986) suggesting in-situ fragmentation during rapid fluid pressure drops that developed during fracture dilatancy. Synthetic (R1) and antithetic (R2) Riedel shears are evident from the angles they enclose with the surrounding mylonites (i.e. 15–20° and ca. 80°, respectively) and, in the case of synthetic R1 Riedel shears, from the displacement of minerals such as feldspar porphyroclasts or zircon (Kisters et al., 1997b, 1998). Both R1 and R2 Riedel shears are decorated by elongate to ovoid sulphide grains that are, in places, closely associated with small grains (< 20 μm) of native gold. Dilational jogs are manifested by their ideally rhomb-shaped geometries

(Fig. 5c). They occur along and/or between subparallel pairs of synthetic Riedel shears or preferentially along the contacts between bounding mylonites and lithons. Dilational jogs also contain mm-size implosion breccias of wall-rock material. In addition to these geometrically fairly regularly distributed features, more competent minerals such as feldspar porphyroclasts or magnetite grains may be fractured showing sulphide-filled cracks of variable, but commonly high-angle orientation. Roughly orthogonal vein sets show planar fracture geometries with large aspect ratios. They tend to be approximately parallel and perpendicular to enveloping mylonites and are lined with fine specks of native gold and sulphides together with quartz, alkali feldspar and biotite from the main alteration paragenesis.

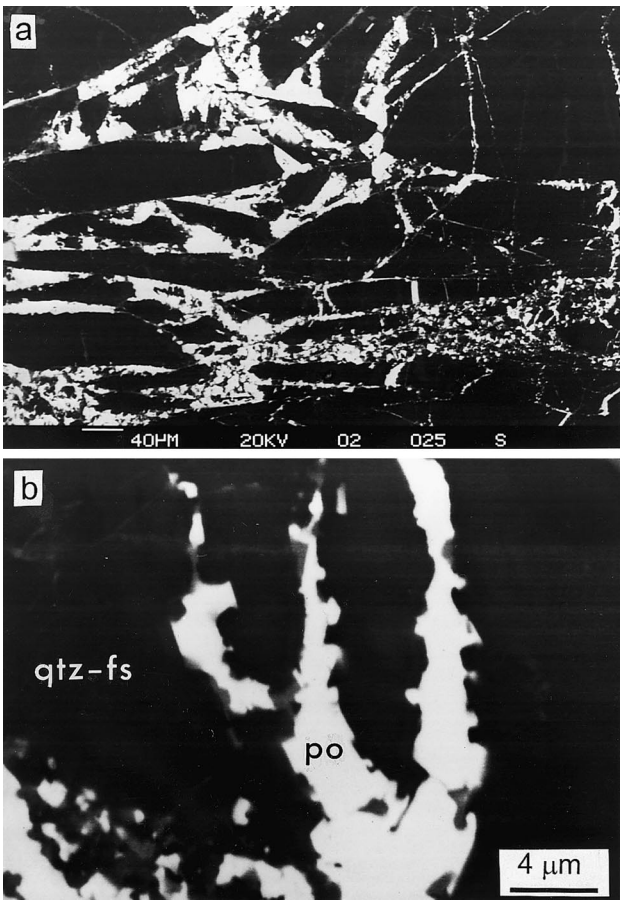


Fig. 6. Back scattered SEM photograph of an implosion breccia contained in lithons showing the angular shape of fragments consisting of mainly quartz and feldspar from the main alteration paragenesis (black) cemented by sulphides (mainly pyrrhotite, light). Note that fracture surfaces bounding the fragments are not straight but display somewhat serrated outlines. (b) Detail of the fracture surface bounding the angular fragments showing positive topological features that cannot be matched across the fractures. Positive topological features are euhedral crystals of feldspar and quartz indicating the fractures had remained open during growth of the crystals, probably due to the presence of a lithostatically pressured fluid phase (see text for further discussion).

#### *3.4.3. Relative timing of fracture formation and deformation*

The structural siting of sulphides described above illustrates that sulphide mineralisation may be hosted by structures related to high-temperature ductile shearing (Fig. 5a, b) as well as in brittle structures, mainly preserved in lithons (Fig. 5c–e). Most vein geometries are mutually cross-cutting which, together with the fact that veins contain similar high-temperature mineral parageneses, implies that different vein sets formed over a time interval during which conditions did not change significantly. Although numerous veins appear to be intact, most veins are variably deformed and vein segments are folded, rolled, transected by microscopic shear veins and microfaults or sheared out in the plane of the mylonitic foliation. Moreover, sulphide veins in lithons show a systematic occurrence and geometry as sets of Riedel shears or tension gashes whose orientation relates to the geometry and kinematics of bounding mylonites. The sum of these features indicates that there were many episodes of veining and, significantly, that veining and brittle fracturing occurred during ductile shearing.

### *3.5. Topology of fracture surfaces in lithons*

In sulphide veins that are only weakly affected by post-depositional deformation, fracture surfaces bounding fragments appear to be straight, giving rise to angular fragments and breccia textures. At higher magnification and viewed with SEM, however, fracture surfaces are not smooth and can be seen to be highly irregular, commonly displaying a zigzag pattern of short and straight segments (Fig. 6a, b). These irregularities along fracture surfaces are caused by euhedral grains of quartz and alkali-feldspar that have grown on the walls of now sulphide-filled fractures (Fig. 6b). Notably, crystals are without a matching topology on the facing surface which, together with their euhedral form, requires that they had free space to develop.

### *3.6. Connectivity of fractures*

The connectivity of fracture porosities is evidenced by the intersection of the different fracture geometries. If closely spaced, R1 and R2 Riedel shear fractures may form wire-mesh-like patterns that enclose lozenge-shaped wall-rock fragments. The highest fracture abundance and closest spacing of sulphide-filled fractures is commonly observed along the upper and lower bounding contacts of the lithons indicating that brittle–ductile deformation and high strain rates were concentrated along the lithon–mylonite interface. The

Table 1
Whole-rock geochemical analyses of samples used for the isocon diagrams presented in Fig. 7

| Reef type | | Shallow reef | | | | | | Steep reef | | | | |
|---|---|---|---|---|---|---|---|---|---|---|---|---|
| Sample no. | | 3/7 | 3/7 | K16 | K14 | K9 | K6 | 30/3 | 30/2 | K23 | K22a | K20a |
| Sample | | Enderbite | Mylonite | Enderbite | Lithon | Migmatite | Massive lithon | Enderbite | Mylonite | Enderbite | Lithon | Massive lithon |
| $SiO_2$ | % | 65.28 | 65.07 | 69.18 | 56.74 | 70.29 | 10.91 | 74.68 | 73.53 | 60.68 | 65.08 | 41.51 |
| $TiO_2$ | % | 0.62 | 0.58 | 0.57 | 0.85 | 0.49 | 0.03 | 0.24 | 0.36 | 0.86 | 0.71 | 0.93 |
| $Al_2O_3$ | % | 17.08 | 16.42 | 15.36 | 12.30 | 14.73 | 0.75 | 13.59 | 14.40 | 16.28 | 15.75 | 6.62 |
| FeO | % | 4.38 | 4.60 | 3.90 | 13.03 | 3.99 | 51.26 | 1.54 | 2.00 | 7.76 | 5.72 | 24.07 |
| MnO | % | 0.07 | 0.13 | 0.06 | 0.06 | 0.06 | n.d. | 0.04 | n.d. | 0.13 | 0.10 | 0.13 |
| MgO | % | 1.65 | 1.42 | 1.06 | 1.52 | 1.30 | 0.28 | 0.55 | 0.71 | 3.33 | 2.29 | 1.13 |
| CaO | % | 5.36 | 5.68 | 4.53 | 1.64 | 4.96 | 0.06 | 2.34 | 2.67 | 7.42 | 5.02 | 2.51 |
| $Na_2O$ | % | 3.81 | 3.38 | 3.52 | 1.63 | 3.62 | n.d. | 3.41 | 3.35 | 3.78 | 3.59 | 1.49 |
| $K_2O$ | % | 1.32 | 1.39 | 1.55 | 6.01 | 0.67 | 0.15 | 4.05 | 3.64 | 0.70 | 1.04 | 0.45 |
| $P_2O_5$ | % | 0.13 | 0.11 | 0.15 | 0.08 | 0.11 | 0.02 | 0.07 | n.d. | 0.16 | 0.13 | 0.28 |
| S | % | 0.01 | 0.04 | 0.02 | 4.74 | 0.08 | 33.04 | 0.11 | 0.20 | 0.03 | 0.37 | 18.08 |
| $CO_2$ | % | 0.11 | 0.52 | 0.09 | 0.05 | 0.12 | 0.06 | 0.07 | 0.09 | 0.14 | 0.18 | 0.17 |
| $H_2O$ | % | 0.50 | n.d. | 0.50 | 0.60 | n.d. | 1.78 | 0.50 | 0.59 | 0.50 | 1.23 | 1.44 |
| Total | % | 100.34 | 99.32 | 100.48 | 99.25 | 100.42 | 98.33 | 101.20 | 101.54 | 101.78 | 101.21 | 98.81 |
| density | | | | | | | | | | | | |
| | $g/cm^3$ | 2.73 | 2.67 | 2.71 | 2.86 | 2.77 | 4.17 | 2.63 | 2.68 | 2.83 | 2.77 | 3.24 |
| V | ppm | 86 | 88 | 52 | 90 | 47 | 3 | 16 | 23 | 152 | 96 | 10 |
| Cu | ppm | 7 | 10 | 21 | 4250 | 66 | 1028 | 8 | 145 | 48 | 1394 | 3525 |
| Au | ppb | 9 | 73 | 56 | 2410 | 54 | 172 | 10 | 272 | 47 | 253 | 716 |
| Hf | ppm | 4 | 4 | 6 | 3 | 6 | 1 | 5 | 11 | 5 | 3 | 2 |
| Zr | ppm | 142 | 150 | 235 | 98 | 211 | 44 | 156 | 388 | 173 | 110 | 85 |
| Y | ppm | 26 | 16 | 18 | 12 | 17 | 6 | 10 | 5 | 34 | 16 | 24 |
| La | ppm | 24.4 | 20.7 | 34.5 | 14.9 | 22.4 | 2 | 34.1 | 21.6 | 24.9 | 20.1 | 17 |
| Ce | ppm | 49 | 39 | 64 | 27 | 41 | 6 | 66 | 34 | 60 | 41 | 44 |
| Nd | ppm | 20 | 11 | 14 | 8 | 10 | n.d. | 24 | 12 | 26 | 14 | 15 |
| Sm | ppm | 4.5 | 2.7 | 3.4 | 1.9 | 2.8 | 0.4 | 3.5 | 1.4 | 5.5 | 2.6 | 3.8 |
| Eu | ppm | 1.1 | 1 | 1.1 | 1 | 0.9 | 0.3 | 0.7 | 1.2 | 1.2 | 0.9 | n.d. |
| Yb | ppm | 2.5 | 1.8 | 2.1 | 1.6 | 1.9 | n.d. | 1.3 | 0.7 | 3.3 | 2.1 | 1.4 |

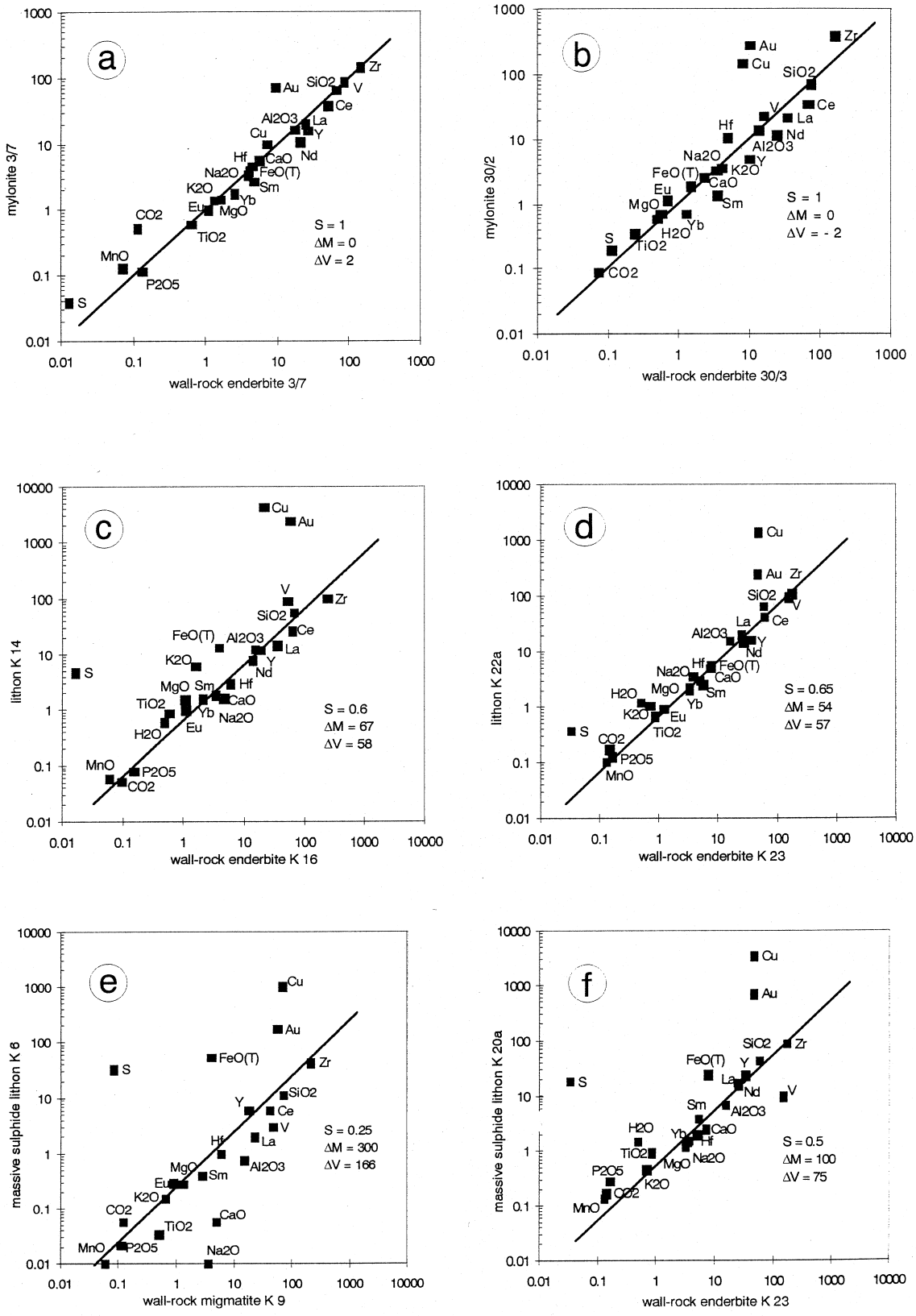


Fig. 7. (*Caption overleaf*).

abundance and spacing of fractures decreases markedly towards the centre of individual lithons. Once sulphide-filled cracks have formed an interconnected network, fragments of wall rocks and alteration parageneses form subangular to rounded porphyroclasts and the resulting textures in massive sulphide ores are locally referred to as 'pebbly-' or 'breccia ores'. In these massive sulphide ores, the geometry and orientation of fractures can no longer be identified and the resulting textures resemble 'Durchbewegungs' textures (after Ramdohr, 1975), although primary sulphide textures are obscured by the pervasive static recrystallisation of sulphides. Durchbewegungs-like textures are probably due to the weak nature of sulphides under the high-grade metamorphic conditions that are likely to form an 'interconnected weak layer' structure (Handy, 1990). Evidence of the weak nature of massive sulphide ores and possibly high finite strains in massive sulphide lithons is also provided by the presence of rounded quartz porphyroclasts, that form rigid and occasionally fractured clasts surrounded by sulphides. Notably, even massive sulphide lithons contain no more than 75–80 vol.% sulphides, which appears to provide an upper limit for the formation of brittle fracture networks in lithons, above which the formation of sulphide-filled fractures in lithons is no longer observed.

## 4. Geochemistry of the reefs

In order to quantify chemical variations associated with deformation and to estimate the nature of fluid–rock interaction, whole-rock geochemical analyses of samples from mylonites and lithons of the reef structures and wall rocks, as a reference, were used. Whole-rock X-ray fluorescence analysis, INAA, and ICP of major, minor, and trace elements were performed on samples from a steep and a shallow reef (Table 1). Samples include the main lithotypes of the shear zones described above, namely wall-rock enderbites, quartz–feldspar–biotite–hornblende mylonites, lithons (containing 15–20 vol.% sulphides) and massive sulphide lithons (containing $\geq 50$ vol.% sulphides).

In the following we have used the isocon method of Grant (1986) to evaluate whether the compositional changes involved significant elemental and/or volumetric gains or losses (Fig. 7). Fig. 7 plots each of the analysed elements in the unaltered wall-rock enderbites vs. quartz–feldspar mylonites, lithons and massive sulphide lithons in double-logarithmic plots following the suggestions of Baumgartner and Olsen (1995). Rock-forming elements are plotted as oxides (except for S) and Fe is plotted as FeO (total), since most Fe is likely to be bound as ferric iron in sulphides and/or biotite in the reefs as is indicated by the petrographic work. Relatively immobile elements that define the isocon line commonly include $Al_2O_3$, $TiO_2$, Zr, together with some High Field Strength and Rare Earth Elements (Selverstone et al., 1991; Leitch and Lentz, 1994). Once this reference frame of immobile elements has been established, geochemical variations can be discussed in terms of element mobility (i.e. as gains or losses of elements). Elements that plot above the isocon are enriched during deformation and alteration, whereas elements that plot below the reference isocon are depleted with respect to the chosen reference frame (Grant, 1986).

Lithotypes from steep and shallow reefs show similar geochemical trends, as is also suggested by the similar petrographic development of shear zone rocks from the two reef geometries. Isocon diagrams of quartz–feldspar–biotite–hornblende mylonites vs. wall rocks (Fig. 7a, b) show that most elements fall on a straight line that defines the isocon. Since most elements are closely clustered around the isocon, a very limited element mobility and largely isochemical behaviour of the mylonites during shearing and predominantly crystal-plastic deformation is suggested. There is only a slight enrichment of Au, Cu, and S as well as $CO_2$ in mylonites compared to wall-rock enderbites which, together with the hydration of mafic minerals (i.e. orthopyroxene replaced by biotite and/or hornblende), provides evidence of a fluid infiltration during deformation.

In lithons, the isocon is well defined by immobile elements such as $TiO_2$, $P_2O_5$, $Al_2O_3$, Zr, Eu, Hf, Nd, Y, and Ce for sample K22a, but less defined for sample K14 (Fig. 7c, d). The latter suggests some degree of mobility of elements that are commonly regarded as being immobile. However, in both lithon samples, a marked shift of the isocon can be seen showing slopes of 0.65 (K22a) and 0.6 (K14), respectively, illustrating

Fig. 7. Element abundances for different reef lithologies vs. wall-rock enderbites and migmatites plotted in double-logarithmic isocon diagrams. $S$: slope of isocon; $\Delta M$: mass change; $\Delta V$: volume change. Isocon diagram for quartz–feldspar–biotite–hornblende mylonite (sample 3/7) from a shallow reef vs. wall-rock enderbite (a) and a steep reef (sample 30/2) (b); (c) isocon diagram for a sulphide-rich lithon (sample K14) vs. wall-rock enderbite from a shallow reef and (d) for a sulphide-rich lithon (sample K22a) vs. wall-rock enderbite; (e) isocon diagram for a massive sulphide lithon (sample K6) vs. wall-rock migmatite from a shallow reef and (f) for a massive sulphide lithon (sample K20a) vs. wall-rock enderbite. Note the dramatic mass and volume gains from largely isovolumetric quartz–feldspar–biotite–hornblende mylonites (a, b), via sulphide-rich lithons (c, d) to massive sulphide lithons (e, f). Geochemical analyses of the samples are given in Table 1.

an enrichment of elements such as S, FeO (T), $SiO_2$, and $K_2O$. Enrichment is most pronounced for Au and Cu. Gains in S and FeO (T) clearly reflect the sulphide mineralisation in the lithons, while increases in $K_2O$ and $SiO_2$ are probably due to the formation of biotite and alkali feldspar and a slight silicification. In contrast to mylonites and lithons, an immobile element isocon for massive sulphide lithons is not always readily identifiable. In sample K20a, an isocon is defined by Zr, Y, La, Nd, and Yb, but is only poorly defined for sample K6 by elements such as $P_2O_5$, Eu, Hf, Y, Ce, and Zr (Fig. 7e, f). Despite these uncertainties, the slope of the isocons is markedly lower (Fig. 7e, f) implying pronounced enrichment of elements that is particularly prominent for S, FeO (T), Au, and Cu. $Na_2O$, CaO, and $Al_2O_3$ are depleted and elements such as $TiO_2$, $SiO_2$, $P_2O_5$, and MnO display contrasting trends in the two massive sulphide lithons analysed, indicating complex fluid–rock interaction. Significantly, Au is markedly enriched in both mylonites and lithons of the auriferous reef structures, but lithons show consistently higher Au values on a mine scale (average 22.5 ppm, $n = 33$ samples) compared to mylonites (average 2.5 ppm, $n = 10$ samples).

In order to quantify the volume (and mass) increase we have used the relationship for volume changes given by Grant (1986):

$$\Delta V = ((1/S)(\rho^a/\rho^o)-1) \times 100, \quad (1)$$

$$\Delta M = ((1/S)-1) \times 100, \quad (2)$$

where $S$ is the slope of the immobile isocon, $\Delta V$ and $\Delta M$ are losses or gains in percent of an element and $\rho^a/\rho^o$ is the ratio for the specific density of altered rock and unaltered protolith, respectively. The specific density (g/cm$^3$) of each sample was determined using the Archimedes principle.

For quartz–feldspar–biotite–hornblende mylonites (Fig. 7a, b), the immobile element isocon has a slope of 1 so that mylonitisation was evidently not associated with any significant volume and/or mass changes. For lithons, the slope of the immobile isocon is 0.6 and 0.65, respectively (Fig. 7c, d), which translates to considerable volume gains of 58% and 57% and corresponding mass gains of 67% and 54%. For massive sulphide lithons, the tentatively constructed immobile isocon has a slope of 0.25 (Fig. 7e) and 0.5 (Fig. 7f). Using Eqs. (1) and (2) the corresponding volume gains are 166% and 75%, respectively, and mass increases are 300% and 100%.

It should be emphasised that these values have to be viewed with caution and most likely represent trends and, at best, approximations of the actual volume and mass changes due to uncertainties in the definition of an immobile element isocon.

## 5. Stable isotopes

In order to obtain information on the nature of fluid–rock interaction in various lithotypes of the reef structures, whole-rock samples and mineral separates were analysed for their $^{18}O/^{16}O$ ratios using the method of Clayton and Mayeda (1963). Mass spectrometric measurements have been performed on a SIRA 9 triple collector instrument of VG-Isogas at the University of Bonn. The data given in the usual δ-notation vs. SMOW are presented in Table 2 and most values represent averages of at least two analyses of the same sample. All duplicates gave an average deviation from the mean of 0.1‰. Several samples had to be treated with diluted HCl prior to isotopic analysis since sulphide contamination in silicate samples is known to cause fractionation in oxygen isotopic compositions. Massive sulphide lithons with up to 60 vol.% sulphides were also analysed, but large errors in the resulting data prohibit clear interpretation and have been rejected in most cases.

The magmatic origin of the rocks at Renco is evidenced by whole-rock $\delta^{18}O$ values that show a small range of 6.9 and 8.5‰. Wall-rock enderbites have values of ca. 7‰ and 8‰ for whole-rock and quartz-mineral separates, respectively. The quartz–feldspar–biotite–hornblende mylonite of sample 30/2 is similar in its isotopic composition to enderbites. In contrast all lithotypes from the mineralised shear zones, except for sample 30/2, show a marked shift of $\delta^{18}O$ whole-rock values and for quartz-mineral separates compared to wall-rock enderbites and quartz–feldspar–biotite–hornblende mylonites (Fig. 8). The whole-rock $\delta^{18}O$ value of the mineralised lithon sample K14 represents an exception to this general trend, possibly because of fractionation effects due to the high sulphide content of the sample. The increase in $\delta^{18}O$ whole-rock and quartz values from close to 7–8‰ for the enderbites to > 8–9‰ in the quartz–mylonites and lithons suggests, in general, open system behaviour during deformation

Table 2
Compilation of $\delta^{18}O$ values for whole rocks and quartz from different lithotypes within the reef structures (compare Fig. 8)

| Sample | $\delta^{18}O$ Whole rock | $\delta^{18}O$ Quartz |
|---|---|---|
| Enderbite K1 | 6.9 | 7.7 |
| Enderbite K23 | 7.0 | 7.7 |
| Enderbite K33 | 7.1 | 8.2 |
| Qtz–fs–bt–hbl–mylonite 30/2 | 7.5 | 7.8 |
| Qtz–mylonite 27/7 | 8.55 | 8.8 |
| Qtz–mylonite K21 | 8.1 | 8.2 |
| Mineralised lithon K20 | 8.5 | 8.4 |
| Mineralised lithon K14 | 7.0 | 9.2 |
| Massive sulphide lithon 29/3 | – | 9.2 |

and fluid flow. Notably, the quartz–feldspar–biotite–hornblende mylonite of sample 30/2, which is affected only by retrograde shear deformation, is similar in its isotopic composition to enderbites and less enriched in $^{18}O$ than the quartz–mylonites and lithons. The small isotopic shift of mylonite sample 30/2 indicates that parts of the shear zones have been less affected by pervasive fluid flow, while others, namely quartz–mylonites and lithons record larger fluid fluxes. These results tie in with the petrographic results and mass balance calculations presented above that indicate strongly heterogeneous fluid flow within the shear zones, implications of which are discussed below.

## 6. Discussion

### 6.1. Mass transfer

The data presented above show that the shear zones of the Renco mine display a characteristic structural partitioning comprised of two distinct domains, namely high-temperature mylonites and brittle–ductile lithons. Mineral and isotope thermometry indicate that deformation and associated fluid flow have occurred contemporaneously in mylonites and lithons. The markedly different petrographic, geochemical and isotopic variability of the two domains suggests a very heterogeneous mass transfer in the narrow reefs that is, in all likelihood, a reflection of a heterogeneous permeability structure as will be discussed in the following paragraphs.

Quartz–feldspar–biotite–hornblende mylonites in the reefs have evidently formed during progressive deformation of wall-rock enderbites during retrograde, amphibolite-facies conditions. Evidence for the creation of permeability during ductile shearing and dynamic recrystallisation is provided by fine-grained sulphides and newly grown biotite (bt II) that are mainly confined to recrystallised mantles of feldspar porphyroclasts or in finely recrystallised shear bands within mylonites (Fig. 4a). The presence of sulphide-filled fractures in feldspar porphyroclasts suggests that microscopic and macroscopic fracture permeability have, at least partly, contributed to the overall permeability of mylonites. However, the largely immobile behaviour of major elements and the lack of considerable volume and/or mass increases in mylonites indicates that fluid infiltration during mylonitisation was probably limited. This is consistent with the subordinate gold-sulphide mineralisation, the presence of relictic orthopyroxene, the lack of pervasive alteration assemblages and similar $\delta^{18}O$ signatures of mylonites compared to wall-rock enderbites.

Although quartz mylonites are only locally developed, they form a common constituent of the reef structures, showing similar outcrop patterns and gradual lateral transitions with the more common quartz–feldspar–biotite–hornblende mylonites. The local development of quartz mylonites is interpreted to have formed during transient episodes of synkinematic quartz-vein formation in the shear zones. During progressive deformation, quartz veins underwent pervasive dynamic recrystallisation and were transposed into the mylonitic fabric yielding essentially quartz mylonites as documented by, e.g., McCuaig and Kerrich (1994) for amphibolite-facies auriferous shear zones in Canada and Australia. Synkinematic quartz veining is also suggested by the shifts in $\delta^{18}O$ values compared to wall rocks and quartz–feldspar–biotite–hornblende mylonites. Notably, $\delta^{18}O$ values of quartz in quartz mylonites are similar to those of quartz in lithons. The detailed process of quartz mylonite formation is not well understood at this point. The presence of strongly folded or drawn out quartz ribbons and veinlets in lithons and quartz porphyroclasts in massive-sulphide lithons possibly indicates that quartz veining occurred prior to the formation of lithons.

Significant volume and mass gains, associated element mobility and consistently higher Au-grades compared to enveloping mylonites, the formation of the distinct garnet–biotite–quartz–alkali feldspar $\pm$ siderite alteration mineral paragenesis and isotopic signatures suggest that lithons in the reefs were sites of extensive advective fluid flow. The progressive volume and mass gains correlate with the development of fracture dilatancy and accompanying precipitation of hydrothermal minerals in lithons. Textural and petrographic observations indicate that it is mainly the precipitation of sulphides in dilatant sites directly from solution that has caused the dramatic volume and mass gains in lithons.

The massive introduction of elements such as S and Fe together with Au and Cu into lithons in the absence of local sources, the lack of a pronounced wall-rock alteration and the marked shift of $\delta^{18}O$ values of lithons and quartz mylonites compared to wall-rock enderbites and quartz–feldspar–biotite–hornblende mylonites indicates the infiltration of fluids from some distant source rather than small-scale lateral diffusional and/or mechanical segregation. Based on timing relationships between the late-Archaean, regional-scale thrusting of high-grade metamorphic rocks of the Northern Marginal Zone onto the Zimbabwe craton and the widespread amphibolite-facies retrogression of the enderbites and element abundances in the reefs, Kolb et al. (2000) have concluded that the generation of fluids was due to devolatilisation reactions in the overthrusted low- to medium-grade granite–greenstone terrains of the Zimbabwe craton.

The restricted scale and sharp contacts of the

different domains testify to considerable permeability contrasts in the narrow shear zones. Thus, the highly focussed fluid flow confined to lithons and only limited fluid and material transport in mylonites illustrates a pronounced hydrologic segmentation of the narrow shear zones. The hydrologic segmentation is closely coupled with the internal structural development of the shear zones, which has resulted in the juxtaposition of two types of permeability, namely (1) grain-scale permeabilities during predominantly ductile creep in quartz–feldspar–hornblende mylonites, and (2) mainly fracture permeabilities in lithons. Since the shear zones are developed in relatively homogeneous enderbites, lithological controls of the wall rocks of either a chemical or mechanical nature are unlikely to have determined the structural heterogeneity and variability of fluid–rock interaction. We interpret the close spatial relationship between ductile creep in mylonite zones and alternating episodes of fracturing and crystal-plastic deformation in lithons to reflect a pronounced strain partitioning that has resulted in and was augmented by the hydrologic segmentation of the narrow reefs.

### 6.2. Implications for mass transport and rheology of the shear zones

The spatial distribution of mylonites and lithons and accompanying mass transfer patterns are used to formulate a conceptual model for the rheology and mass hydraulic properties of the narrow Renco shear zones.

Implosion breccias and brittle fracturing similar to those observed in the Renco reefs in core material from the Cajon Pass Drill Hole have been related by Blenkinsop and Sibson (1992) to non-steady aseismic creep and gradual fluctuations of shear stress levels and strain rates in areas of distributed deformation. In the Renco reefs, however, strain is strongly partitioned and fracture formation is confined to lithons. Strain partitioning has allowed mylonitic parts of the reefs to deform by aseismic creep, while the formation of brittle fracture sets and breccias in lithons suggests that ductile creep at low stress in mylonites has transferred load to lithons which behaved in a brittle manner. The high fracture abundance along the mylonite–lithon interface indicates transient episodes of localised high strain rates rather than distributed deformation, and brittle fracturing could be associated with seismogenic cycling related to episodes of seismic slip. Cross-cutting relationships illustrate that fracture formation and sealing in lithons were episodic, so that fracture permeability was transient. Seismic slip and coseismic dilatancy induced by the elastic deformation caused rapid fluid movement into cracks following the hydraulic gradient created during fracture events (Sibson, 1986). Hence, dilatant fractures have most likely represented small-scale pumps ('seismic pumps', e.g. Sibson, 1986; Oliver, 1996) that were healed by mainly sulphides probably due to phase separation of the infiltrating fluid during catastrophic fluid pressure drops given the high $H_2S$ activity of the fluid (Kolb et al., 2000). Brittle fracturing under high-grade metamorphic conditions at reasonable geologic strain rates is only possible in the presence of close-to-lithostatic fluid pressures so that the least compressive stress and tensile strength of the rocks can be overcome (e.g.

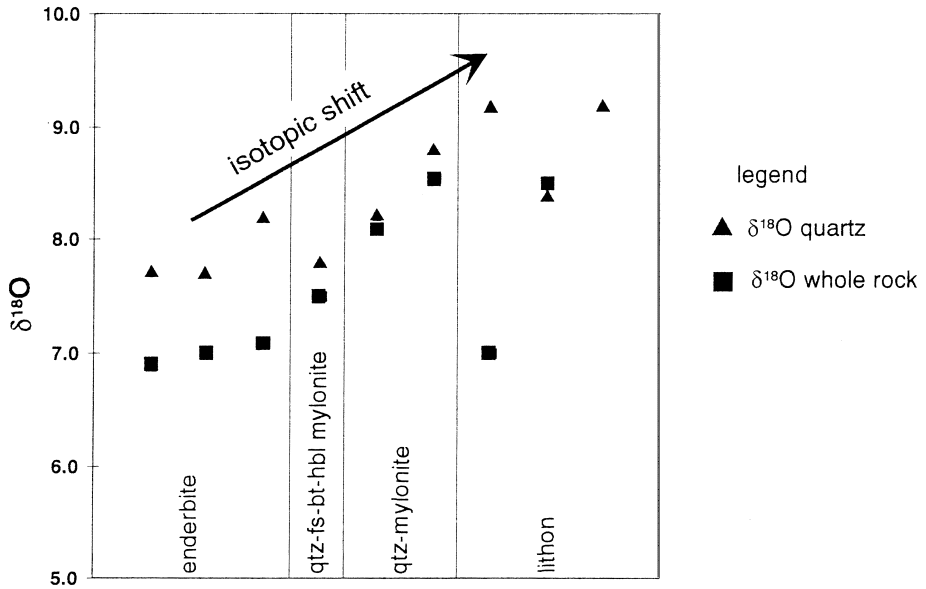


Fig. 8. Histogram of quartz and whole-rock $\delta^{18}O$ values illustrating the isotopic shift from lighter $\delta^{18}O$ values in enderbites and quartz–feldspar–biotite–hornblende mylonites to heavier values in quartz mylonites and lithons.

Etheridge, 1983). The presence of pressurised fluids in lithons is indicated by the growth of euhedral quartz and/or alkali feldspar from the alteration mineral assemblage into sulphide filled fractures (Fig. 6b), Ague (1995) concluded from similar textural relationships in pegmatite dykes that lithostatically pressurised fluids must have been present to maintain open fracture porosity even at high confining pressures in mid- to lower-crustal environments. Elevated fluid pressures in lithons are likely to result from the anastomosing geometry of the enclosing low-permeability mylonites that are, in turn, bounded by largely impermeable enderbitic wall rocks. High-temperature laboratory experiments by Blanpied et al. (1995) have shown that low-permeability seals may form during ductile shearing of artificial faults. In addition, prolonged periods of ductile creep and compaction during interseismic periods will trap and pressurise fluids in lithons. Compaction during ductile creep in the lithons together with the healing of microfractures by hydrothermal phases will result in fairly rapid pressure build-ups, that, together with the low shear strength along the shear zones, allows for a reactivation of the shear zones at low differential stress. In addition, the introduction of relatively weak sulphide phases may localise ductile strain and the resulting high strain rates may cause fracturing of stronger silicate alteration minerals leading, in turn, to increased fracture permeability. The petrographic work indicates, however, that fracture formation appears to be limited to lithons containing $\leq$ 75 vol.% sulphides and that with higher sulphide contents, the rheology of lithons is dominated by the weak sulphide phases.

For shear zones that deform predominantly by ductile creep experimental work by Sleep and Blanpied (1992) suggests that the conditions for seismic slip and brittle failure along fault zones (i.e. fluid pressure build-up to a critical stress state along the fault plane) may be accomplished after merely several tens of years. Repeated elastic failure in the lithons can thus occur over relatively short periods and a fault zone that is active over a reasonable geological time (i.e. $10^4$–$10^6$ y) may undergo between hundreds and thousands of fracturing events as implied by the abundance of overprinting vein geometries in lithons.

The sharp contacts between lithons and mylonites and the spatial distribution of lithons demonstrate that the formation of transient fracture episodes in the shear zones was strongly heterogeneous being largely restricted to well-defined domains of lithons. This has two main implications for the rheology and fluid flow properties in the shear zones. Firstly, it suggests the transport of fluids along discrete fluid channelways or as distinct fluid pockets. Secondly, it would imply the presence of unstable slipping patches, which are in a continuous state of incipient failure within the otherwise ductile shear zones. The formation of discrete fluid pressure compartments in the deeper parts of fault zones has been described by Byerlee (1993), either due to the solution and precipitation of minerals preferably along the contact of the actual fault zones with the country rocks, or due to localised reaction-softening processes (Chester et al., 1993; Wintsch et al., 1995). In case of the high-temperature shear zones of the Renco mine, crystal-plastic deformation and ductile creep in low-permeability mylonite bands would represent pressure seals bounding highly pressurised and isolated lithons.

The extensive fluid throughflow that is required for the formation of an economic-grade gold mineralisation such as that of Renco is highly dependent on the presence of suitably interconnected porosities and larger-scale fluid advection will only be triggered if two different hydraulic pressure regimes are connected by the shear zone (e.g. Ridley, 1993; Knipe and McCaig, 1994). Hence, the geometry and interconnection of high-permeability pathways on the scale of metres to hundreds of metres is critical for the initiation of fluid flow in a shear zone system (see e.g. Oliver, 1996, for the discussion of scales of permeability). As discussed in the foregoing paragraphs, the auriferous shear zones at Renco represent relatively closed entities that experienced only limited fluid advection from adjacent wall rocks. Yet, the petrographic, geochemical and isotope data suggest that large amounts of fluids have been channelised through the lithons. Underground exposures show a coalescence of macrolithons predominantly in an up-dip direction, i.e. in the direction of the tectonic transport while the coalescence of reefs is less common parallel to the strike of the reef structures. The breaching of adjacent fluid conduits (i.e. lithons) is determined by the anastomosing geometry of the enveloping mylonites, which thus provides a network of narrow, interconnected high-permeability domains on a large scale.

## 7. Conclusions

The petrographic, structural, geochemical and isotopic data presented above indicate the following points with respect to deformation and the hydraulic properties of the Renco reef structures:

1. Structural evidence indicates that ductile creep and microscopic and macroscopic brittle fracturing have proceeded simultaneously in mid- to upper amphibolite-facies shear zones of the Renco mine.
2. The preservation of sulphide-filled, interconnected fracture networks in lithons, associated massive volume and mass increases related to the precipitation of hydrothermal minerals, and shifts in the isotopic signature of lithons compared to mylonites

and enderbites indicates that fracture permeabilities in the mylonitic shear zones were the dominant mechanism for the generation of permeabilities. In contrast, grain-scale permeability during crystal-plastic deformation in mylonites has evidently resulted in only limited fluid advection.

3. Given the restricted scale and sharp contacts of high- and low-permeability domains, fluid flow was strongly domainal and indicates a strong hydrologic segmentation of the shear zones. It thus appears that fluids have migrated as distinct shear-zone parallel fluid pockets. The breaching of individual fluid pockets provides a three-dimensional, interconnected network of high-permeability domains within the narrow shear zones. Since these high-permeability domains are effectively sealed off from the wall rocks, far-field fluid transport of externally derived fluids is possible.
4. The spatially irregular distribution of lithons within the mylonitic shear zones implies the existence of localised zones that are in a continuous state of incipient failure due to high pore-fluid pressures. This indicates that deformation in mid-crustal, ductile shear zones may not be characterised by continuous, aseismic creep, but rather by irregularly distributed domains of localised and transiently occurring seismic slip and rupture. Deep-crustal seismicity is a widely documented feature (e.g. Deichmann, 1992) and deformation mechanisms such as those described for the Renco shear zones may contribute to low-magnitude seismic events in the middle and lower continental crust.
5. Fracture networks that account for the bulk of permeability in ductile shear zones are likely to be far more widespread than commonly observed. However, the recognition of syndeformational fracture events in mid-crustal shear zones may be severely hampered due to the progressive overprinting of brittle fabrics during prolonged periods of ductile creep (e.g. Knipe and McCaig, 1994; McCaig, 1997), the absence of readily identifiable vein fillings or lower degrees of strain partitioning that would have preserved distinct structural domains within the shear zones. An important consequence of the potentially heterogeneous nature of ductile shear zones as demonstrated in this study is that geochemical work and mass balance calculations on mylonites should be carried out with great care since the complex flow patterns may easily be overlooked or underestimated.

## Acknowledgements

The authors thank the mine management of the Renco mine for the permission to publish the results of this study and the mine geologists for their support during the underground work. Stephan Kaufhold and Ute Müller are thanked for drafting the figures and Monika Wiechert for photographic work. Comments by Alice Post on an earlier version of the manuscript are greatly appreciated. The manuscript greatly benefited from insightful reviews by Siyanda Mkweli and John Ridley and editorial comments by Tom Blenkinsop. Financial support of this study by the Deutsche Forschungsgemeinschaft (DFG grant Me 1425/1-1, 1–2) is gratefully acknowledged.

## References

Ague, J.J., 1995. Deep crustal growth of quartz, kyanite and garnet into large-aperture, fluid-filled fractures, north-eastern Connecticut, USA. Journal of Metamorphic Geology 13, 299–314.

Baumgartner, L.P., Olsen, S.N., 1995. A least-square approach to mass transport calculations using the isocon method. Economic Geology 90, 1261–1270.

Berger, M., Kramers, J.D., Naegler, T.F., 1995. Geochemistry and geochronology of charnoenderbites in the northern marginal zone of the Limpopo Belt, southern Africa, and genetic models. Schweizerische Mineralogische und Petrographische Mitteilungen 75, 17–42.

Blanpied, M.L., Lockner, D.A., Byerlee, J.D., 1992. An earthquake mechanism based on rapid sealing of faults. Nature 358, 574–576.

Blanpied, M.L., Lockner, D.A., Byerlee, J.D., 1995. Frictional slip of granite at hydrothermal conditions. Journal of Geophysical Research 100, 13045–13064.

Blenkinsop, T.G., Rollinson, H.R., 1992. North Limpopo workshop field guide and abstracts volume. Harare, Geological Society of Zimbabwe, 56 pp.

Blenkinsop, T.G., Sibson, R.H., 1992. Aseismic fracturing and cataclasis involving reaction softening within core material from the Cajon Pass drill hole. Journal of Geophysical Research 97, 5135–5144.

Blenkinsop, T.G., Frei, R., 1996. Archean and Proterozoic mineralization and tectonics at the Renco mine (Northern Marginal Zone, Limpopo Belt, Zimbabwe). Economic Geology 91, 1225–1238.

Blenkinsop, T.G., Mkweli, S., Rollinson, H.R., Fedo, C.M., Paya, B.K., Kamber, B., Kramers, J.D., Berger, M., 1995. The North Limpopo Thrust Zone (NLTZ): The northern boundary of the Limpopo belt in Zimbabwe and Botswana. Abstracts of Proceedings, Centennial Geocongress, Geological Society of South Africa Extended Abstracts 1, 174–177.

Byerlee, J., 1993. Model for episodic flow of high-pressure water in fault zones before earthquakes. Geology 21, 303–306.

Chester, F.M., Evans, J.P., Biegel, R.L., 1993. Internal structure and weakening mechanisms of the San Andreas fault. Journal of Geophysical Research 98, 771–786.

Clayton, R., Mayeda, T.K., 1963. The use of bromine pentafluoride in the extraction of oxygen from oxides and silicates for isotopic analysis. Geochimica Cosmochimica Acta 27, 43–52.

Cox, S.F., Etheridge, M.A., 1989. Coupled grain-scale dilatancy and mass transfer during deformation at high fluid pressures: examples from Mount Lyell, Tasmania. Journal of Structural Geology 11, 147–162.

Deichmann, N., 1992. Structural and rheological implications of lower-crustal earthquakes below northern Switzerland. Physics of the Earth and Planetary Interiors 69, 270–280.

Dipple, G.M., Ferry, J.M., 1992. Metasomatism and fluid flow in

ductile fault zones. Contributions to Mineralogy and Petrology 112, 149–164.

Etheridge, M.A., 1983. Differential stress magnitudes during regional deformation and metamorphism: upper bound imposed by tensile fracturing. Geology 11, 231–234.

Etheridge, M.A., Wall, V.J., Cox, S.F., Vernon, R.H., 1984. High fluid pressures during regional metamorphism and deformation: implications for mass transport and deformation mechanisms. Journal of Geophysical Research 89, 4344–4358.

Evans, J.P., Chester, F.M., 1995. Fluid–rock interaction in faults of the San Andreas system: Inferences from San Gabriel fault rock geochemistry and microstructures. Journal of Geophysical Research 100, 13007–13020.

Ferry, J.M., Spear, F.S., 1978. Experimental calibration of the partitioning of Fe and Mg between biotite and garnet. Contributions to Mineralogy and Petrology 66, 113–117.

Goddard, J.V., Evans, J.P., 1995. Chemical changes and fluid–rock interaction in faults of crystalline thrust sheets, northwestern Wyoming, U.S.A. Journal of Structural Geology 17, 533–547.

Grant, J.A., 1986. The isocon diagram—a simple solution to Gresens' equation for metasomatic alteration. Economic Geology 18, 1976–1982.

Handy, M.R., 1990. The solid-state flow of polymineralic rocks. Journal of Geophysical Research 95, 8647–8661.

Kamber, B.S., Kramers, J.D., Napier, R., Cliff, R.A., Rollinson, H.R., 1995. The Triangle shear zone, Zimbabwe, revisited: New data document an important event at 2.09 Ga in the Limpopo Belt. Precambrian Research 70, 191–213.

Kisters, A.F.M., Kolb, J., Meyer, F.M., 1997a. Archean and Proterozoic mineralization and tectonics at the Renco Mine (Northern Marginal Zone, Limpopo Belt, Zimbabwe)—A Discussion. Economic Geology 92, 745–746.

Kisters, A.F.M., Meyer, F.M., Ebeling, J., 1997b. Permeability enhancement and fluid flow in mid-crustal rocks: The Renco gold mine, southern Zimbabwe. Abstracts to Proceedings, Geofluids II, 247–250.

Kisters, A.F.M., Kolb, J., Meyer, F.M., 1998. Gold mineralization in high-grade metamorphic shear zones of the Renco Mine, southern Zimbabwe. Economic Geology 93, 587–601.

Kolb, J., Kisters, A.F.M., Hoernes, S., Meyer, F.M., 2000. The origin of fluids and nature of fluid–rock interaction in mid-crustal auriferous mylonites of the Renco mine, S-Zimbabwe. Mineralium Deposita 35, 157–168.

Knipe, R.J., McCaig, A.M., 1994. Microstructural and microchemical consequences of fluid flow in deforming rocks. In: Parnell, J. (Ed.), Geofluids: Origin, migration and evolution of fluid in sedimentary basins, Geological Society Special Publication, 78, pp. 99–112.

Leitch, C.H.B, Lentz, D.R. 1994. The Gresens approach to mass balance constraints of alteration systems: methods, pitfalls, examples. In: Lentz, D.R. (Ed.), Alteration and alteration processes associated with ore-forming systems, Geological Association of Canada, Short Course Notes, pp. 161–192.

Mancktelow, N.S., Grujic, D., Johnson, E.L., 1998. An SEM study of porosity and grain boundary microstructure in quartz mylonites, Simplon Fault Zone, Central Alps. Contributions to Mineralogy and Petrology 131, 71–85.

Marone, C., 1998. The effect of loading rate on static friction and the rate of fault healing during the earthquake cycle. Nature 391, 69–72.

Marone, C., Raleigh, C.B., Scholz, C.H., 1990. Frictional behaviour and constitutive modeling of simulated fault gouge. Journal of Geophysical Research 95, 7007–7025.

Marquer, D., Burkhard, M., 1992. Fluid circulation, progressive deformation and mass transfer processes in the upper crust: the example of basement–cover relationships in the External Crystalline Massifs, Switzerland. Journal of Structural Geology 14, 1047–1057.

Marquer, D., Petrucci, E., Iacumin, P., 1994. Fluid advection in shear zones: evidence from geological and geochemical relationships in the Aiguilles Rouges Massif (Western Alps, Switzerland). Schweizerische Mineralogische Petrographische Mitteilungen 74, 137–148.

McCaig, A.M., 1997. The geochemistry of volatile fluid flow in shear zones. In: Holness, M.B. (Ed.), Deformation enhanced fluid transport in the Earth's crust and mantle, The Mineralogical Society Series London, 8, pp. 227–266.

McCuaig, T.C., Kerrich, R. 1994. *P–T–t* deformation fluid characteristics of lode-gold deposits: evidence from alteration systematics. In: Lentz, D.R. (Ed.), Alteration and alteration processes associated with ore-forming systems. Geological Association of Canada, Short Course Notes, pp. 339–379.

Mkweli, S., Kamber, B.S., Berger, M., 1995. A westward continuation of the Zimbabwe craton–northern marginal zone tectonic break and new age constraints on the timing of thrusting. Geological Society of London Journal 152, 77–83.

O'Hara, K., 1988. Fluid flow and volume loss during mylonitization: an origin for phyllonite in an overthrust setting, North Carolina, U.S.A. Tectonophysics 156, 21–36.

O'Hara, K., 1990. State of strain in mylonites from the western Blue Ridge province, southern Appalachians: The role of volume loss. Journal of Structural Geology 12, 419–430.

O'Hara, K., Blackburn, D., 1989. Volume-loss model for trace element enrichments in mylonites. Geology 17, 524–527.

Oliver, N.H.S., 1996. Review and classification of structural controls on fluid flow during regional metamorphism. Journal of Metamorphic Geology 14, 477–492.

Ramdohr, P., 1975. Die Erzmineralien und ihre Verwachsungen, 4th edn. Akademie Verlag, Berlin, 1277p.

Ridley, J.R., 1992. On the origins and tectonic significance of the charnockite suite of the Archean Limpopo belt, northern marginal zone, Zimbabwe. Precambrian Research 55, 407–422.

Ridley, J.R., 1993. The relations between mean rock stress and fluid flow in the crust: with reference to vein- and lode-style gold deposits. Ore Geology Reviews 8, 23–37.

Rollinson, H.R., 1989. Garnet-orthopyroxene thermobarometry of granulites from the North Marginal Zone of the Limpopo Belt, Zimbabwe. In: Daly, J.S., Cliff, R.A., Yardley, B.W.D. (Eds.), Evolution of metamorphic belts, 43. Geological Society of London Special Publication, London, pp. 331–335.

Selverstone, J., Morteani, G., Staude, J.-M., 1991. Fluid channeling during ductile shearing: transformation of granodiorite into aluminous schist in the Tauern Window, Eastern Alps. Journal of Metamorphic Geology 9, 419–431.

Sibson, R.H., 1986. Brecciation processes in fault zones: interferences from earthquake rupturing. Pure Applied Geophysics 124, 159–174.

Sibson, R.H., 1994. Crustal stress, faulting and fluid flow. In: Parnell, J. (Ed.), Geofluids: Origin, migration and evolution of fluid in sedimentary basins, 78. Geological Society Special Publication, pp. 69–84.

Sleep, N.H., Blanpied, M.L., 1992. Creep, compaction and the weak rheology of major faults. Nature 359, 687–692.

Spear, F.S., Peacock, S.M., 1992. Metamorphic Pressure–Temperature–Time Paths. American Geophysical Union, Short Course Notes, 7, 102pp.

Tabeart, C.F., 1989. Structural and geochemical setting of gold mineralization at Renco mine, Zimbabwe. Imperial College, London, 298 pp. PhD-thesis (unpubl.).

Tobisch, O.T., Barton, M.D., Vernon, R.H., Paterson, S.R., 1991. Fluid-enhanced deformation: transformation of granitoids to banded mylonites, western Sierra Nevada, California, and southeastern Australia. Journal of Structural Geology 13, 1137–1156.

Tsunogae, T., Miyano, T., Harris, N.B., 1992. Metamorphic *P–T* profiles from the Zimbabwe craton to the Limpopo belt, Zimbabwe. Precambrian Research 55, 259–277.

Wintsch, R.P., Christofferson, R., Kronenberg, A.K., 1995. Fluid–rock reaction weakening of fault zones. Journal of Geophysical Research 100, 13021–13032.